Phase Transitions and Mechanical Properties of Octahydro-1,3,5,7-tetranitro-1,3,5,7-tetrazocine in Different Crystal Phases by Molecular Dynamics Simulation

Hong-Ling Cui,[†,‡] Guang-Fu Ji,[*,‡,§] Xiang-Rong Chen,[*,†,||] Qing-Ming Zhang,[§] Dong-Qing Wei,[§,⊥] and Feng Zhao[‡]

Institute of Atomic and Molecular Physics, Sichuan University, Chengdu 610064, China, National Key Laboratory of Shock Wave and Detonation Physics, Institute of Fluid Physics, Chinese Academy of Engineering Physics, Mianyang 621900, China, State Key Laboratory of Explosion Science and Technology, Beijing Institute of Technology, Beijing 100081, China, International Centre for Materials Physics, Chinese Academy of Sciences, Shenyang 110016, China, and College of Life Science and Biotechnology, Shanghai Jiaotong University, Shanghai 200240, Shanghai, China

The phase transitions and mechanical properties of the energetic material octahydro-1,3,5,7-tetranitro-1,3,5,7-tetrazocine (HMX) in three pure polymorphs crystals, α-, *β*-, and *δ*-phases, have been studied theoretically. Isothermal−isobaric molecular dynamics (MD) simulations were performed in the temperature range of (5 to 555) K at 0 GPa and the pressure range of (0 to 40) GPa at 298 K. The lattice parameters and volumes show nonlinear dependence on the temperature and pressure. In the high-temperature regime, there exist two phase transitions, that is, from *β*- to α-HMX at 360 K and from α- to *δ*-HMX at 440 K. Under high pressure, the *β*-HMX transition to *δ*-HMX is shown at 27 GPa and 298 K. Within the range of temperature and pressure studies, it can be deduced that the *β*-HMX at lower temperatures and higher pressures, the α-HMX at higher pressures, and the *δ*-HMX at lower temperatures have better malleability.

Introduction

As we all know, HMX[1] (octahydro-1,3,5,7-tetranitro-1,3,5,7-tetrazocine) has been an important and useful energetic material as a secondary explosive since the 1930s. There exhibits four different crystal structures of HMX, three pure crystallization phases, α, *β*, and *δ*, and a hydrate phase *γ*.[2] At ambient conditions, the stabilities of these polymorphs are known to be $\beta > \alpha > \gamma > \delta$.[3] The *β*-HMX phase, with the monoclinic $P2_1/c$ space group, is the most stable form.[4] It has the highest energy and density and the lowest sensitivity at ambient conditions.[4] The *β* crystalline phase has been investigated to contain two $C_4H_8N_8O_8$ groups, and the symmetry axis is *b*, thirteen independent elastic coefficients by X-ray and neutron diffraction.[5,6] The α-HMX phase has been studied to contain eight $C_4H_8N_8O_8$ groups, with the orthorhombic *Fdd*2 space group and nine elastic independent coefficients.[5] The *δ*-HMX phase is formed at the solid−melt interphase in deflagrating HMX, has a hexagonal $P6_122$ structure, *c* symmetry axis, and five independent elastic coefficients, and is considered to be stable at extreme conditions.[7,8] The *γ*-HMX phase has been investigated to contain two $C_4H_8N_8O_8 \cdot 0.5H_2O$ molecules per unit cell, with the *Pn* symmetry space group.[4] Cady and Smith observed two phase transitions; that is, one is the *β*- to α-HMX transition at (375 to 377) K, and the other is the solid α- to *δ*-HMX transformation at (433 to 437) K.[2] Yoo and Cynn[9] found two phase transitions by the diamond-anvil cell, using angle-resolved synchrotron X-ray diffraction and micro-Raman spectroscopy; one is the conformational change at 12 GPa with no apparent volume change, and the other is the phase transformation along with a 4 % volume discontinuity at 27 GPa. Gump and Peiris[10] and Stevens and Eckhardt[11] have studied the compression of *β*-HMX by synchrotron angle-dispersive X-ray diffraction techniques and scattering from a variety of acoustic phonons, respectively. Computational studies were carried out to investigate the influence on the lattice parameters at different pressures or temperatures of *β*-HMX.[12–16] The energetic stabilities and vibrational properties of HMX were simulated by using first principles at different conditions.[17–21]

Despite the above efforts, the phase transition and mechanical properties of three pure polymorphs of HMX crystal have not been explored completely, especially at high pressures and high temperatures. These properties are important to understand HMX crystals. In this work, we carried out molecular dynamics (MD) simulations to study the phase transition and mechanical properties of pure HMX crystals under different temperatures and pressures.

Computational Methods

In this paper the MD simulations were performed with the DISCOVER module of the commercial software Materials Studio.[22] The COMPASS (condensed-phase optimized molecular potentials for atomistic simulation studies) force field[23] was used with a cutoff distance of 10.5 Å. The MD simulations were carried out in the normal pressure and temperature (NPT) ensemble with the Berendsen barostat method[24] and Andersen thermostat method[25] to control the system pressures and temperatures. The simulation supercell contains 96 HMX molecules and 2688 atoms, corresponding to the boxes of $4 \times 4 \times 3$, $3 \times 2 \times 2$, and $4 \times 2 \times 2$ unit cells for the *β*-HMX, α-HMX, and *δ*-HMX, respectively. The initial crystal lattice and atomic position of *β*-HMX, α-HMX, and *δ*-HMX were taken from the experimental results of refs 9, 5, and 8, respectively. The long-range nonbond Coulombic and van der

* To whom correspondence should be addressed. Tel.: +86 816 2485108; e-mail address: cyfjkf@caep.ac.cn (G.-F.J.). Tel.: +86 28 85405516; e-mail address: xrchen@126.com (X.-R.C.).
† Sichuan University.
‡ Chinese Academy of Engineering Physics.
§ Beijing Institute of Technology.
|| Chinese Academy of Sciences.
⊥ Shanghai Jiaotong University.

10.1021/je100009m
Published on Web 03/30/2010

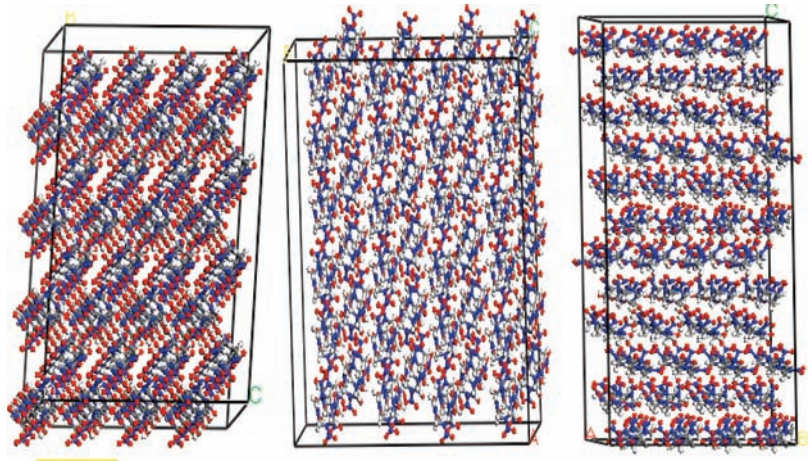

Figure 1. Initial supercell models of HMX in the MD simulation. The left is β-HMX supercell model, the middle is the α-HMX supercell model, and the right is the δ-HMX supercell model.

Table 1. Lattice Parameters Simulated by the COMPASS Force Field Compared with Experimental Values of α, *β*, *δ*-HMX at 298 K and $1.0 \cdot 10^{-5}$GPa

		a	*b*	*c*	α	*β*	*γ*	*V*	*ρ*
		Å			deg			Å^3	g·cm^{-3}
β-HMX	ref 9	6.54	11.05	8.70	90	124.3	90	259.7	1.89
	this work	6.58	11.12	8.76	90	124.3	90	264.9	1.86
α-HMX	ref 5	15.14	23.89	5.91	90	90	90	267.2	1.84
	this work	15.31	24.17	5.98	90	90	90	276.6	1.78
δ-HMX	ref 8	7.71	7.71	32.55	90	90	120	279.4	1.76
	this work	7.76	7.76	32.76	90	90	120	284.7	1.73

Waals interactions were managed using the atom-based summation method.[26] A fixed time step of 1 fs was used in all MD simulations. At each temperature and pressure, the system was first relaxed for $1 \cdot 10^5$ time steps in the equilibration run, followed by a production run of $1 \cdot 10^5$ time steps. The data from the production run were collected for subsequent analysis.

Results and Discussion

Choice of Force Field and Equilibrium of System. Figure 1 displays the supercell models of the crystalline α-, *β*-, and *δ*-HMX in the initial MD simulation. To choose a suitable force field, we carried out a series of tests for *β*-HMX, α-HMX, and *δ*-HMX crystals. The parameters of the COMPASS force field have been tested and confirmed by comparing with the experimental values. The nonbond parameters have been further modified by the thermal physical properties of liquid and solid molecules obtained from the MD method. In previous studies, the COMPASS force field was employed in the MD simulations of many nitramine explosives, such as bicycle-HMX, CL-20, and TNAD.[27–31] The results of MD calculated are listed in Table 1. The discrepancy between our results and the experimental results is small, that is, 0.61 %, 0.63 %, 0.69 %, 2.01 %, and 1.97 % of *a*, *b*, *c*, *V*, and *ρ* for *β*-HMX, 1.12 %, 1.17 %, 1.18 %, 3.54 %, and 3.4 % of *a*, *b*, *c*, *V*, and *ρ* for α-HMX, 0.65 % of *a*, *b*, and *c*, 1.92 % of *V*, and 1.88 % of *ρ* for *δ*-HMX, respectively. The simulated results of geometry parameters are in good agreement with the experiment, indicating that the COMPASS force field is appropriate for simulating the HMX crystal.

Before the statistic analysis, the system must reach the equilibrium state. The equilibrium of the system is achieved when the fluctuations of temperature and the energy are less than 10 %. Typically, the system should achieve its equilibrium in the initial 100 ps, followed by a production run of latter $1 \cdot 10^5$ time steps. It can be seen that the system temperature has reached its equilibrium state within (288 to 308) K (298 ± 10 K) from our results. The amplitudes of fluctuations for potential

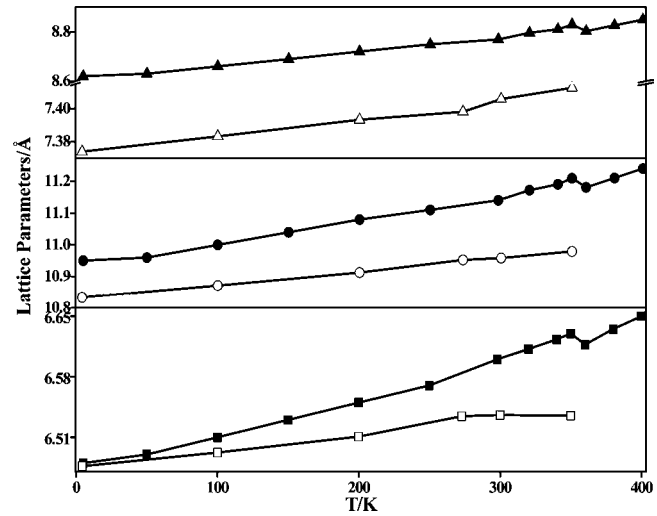

Figure 2. Lattice parameters of *β*-HMX at different temperatures, 0 GPa, in this work and atmospheric pressure in ref 15. ■, *a* in this work, □, *a* in ref 15; ●, *b* in this work; ○, *b* in ref 15; ▲, *c* in this work; △, *c* in ref 15.

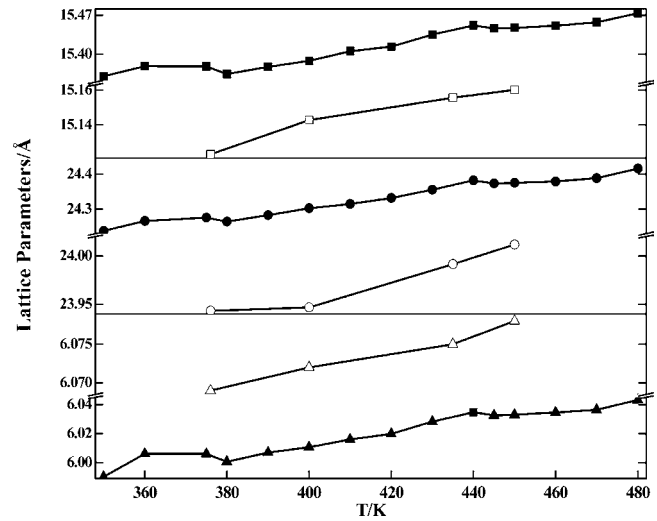

Figure 3. Lattice parameters of α-HMX at different temperatures, 0 GPa, in this paper and atmospheric pressure in ref 15. ■, *a* in this work; □, *a* in ref 15; ●, *b* in this work, ○, *b* in ref 15; ▲, *c* in this work, △, *c* in ref 15.

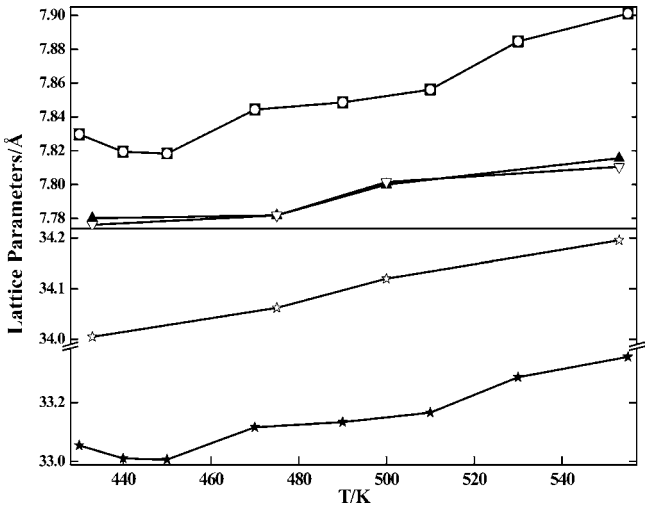

Figure 4. Lattice parameters of δ-HMX at different temperatures, 0 GPa, in this work and atmospheric pressure in ref 15. ■, *a* in this work; ▲, *a* in ref 15; ○, *b* in this work, ▽, *b* in ref 15; ★, *c* in this work, ☆, *c* in ref 15.

energy and nonbond energy are less than 0.3 % and 0.2 %, respectively, showing that the system has reached its energy equilibrium. After equilibration, production runs of 100 ps were then performed.

Phase Transition under Different Temperatures and Pressures. Within NPT ensembles, we calculated the structural properties and phase transition of the β-, α-, and δ-HMX at different temperatures and 0 GPa and at different pressures and 298 K. We simulated the structural properties in the range of (5 to 400) K at 0 GPa and the pressure range of (0 to 31) GPa at 298 K for β-HMX, in the range of (350 to 480) K at 0 GPa and the pressure range of (22 to 40) GPa at 298 K for α-HMX, and in the range of (430 to 555) K at 0 GPa and the pressure range of (20 to 40) GPa at 298 K for δ-HMX.

Under Different Temperatures. Under different temperatures, the lattice parameters and volumes are listed in the Figures 2 to 5 together with the results of ref 15. The lattice parameters and volumes vary nonlinearly with temperature and exhibit an abrupt change at 360 K in the temperature range (5 to 400) K for β-HMX, at (380 and 440) K for α-HMX, and at 440 K for δ-HMX. From Figures 2 to 5, we found two phase transitions: one from β-HMX to α-HMX at (360 to 380) K agrees with the experimental result at (375 to 377) K,[2] and the other from α-HMX to δ-HMX at 440 K agrees with the experimental observation of the phase transition at (433 to 437) K.[2] With temperature increasing the lattice parameters and cell volumes increase, and the crystalline density of three phase decreases gradually in their stable temperature ranges. In the temperature range of (5 to 350) K, the ratio of the change of *a*, *b*, *c*, and *V* are 2.31 %, 2.37 %, 2.44 %, and 7.35 % for β-HMX. Within the range of (380 to 440) K, for α-HMX the changes of lattice parameters are 0.73 %, 0.74 %, and 0.88 % for *a*, *b*, and *c*, respectively; the cell volume change is 2.2 %. For δ-HMX, with temperature increasing from (440 to 555) K, the lattice parameters increase in 0.91 % for *a*, *b*, and *c*, and the cell volume change is 2.7 %. In the corresponding temperature range, the change trend of the lattice parameters and cell volume of our results agree with Sorescu et al.[15] The reason of the discrepancy for β-HMX is that the initial structure is different; the space groups are $P2_1/c$ in our work and $P2_1/n$ for Sorescu et al. Moreover, our results agree with the experimental results well. While, within the entire temperature range considered, the lattice angles almost remain invariant, that is, α and γ are approximately equal to 90° and β remains approximately 124.3° for β-HMX, $\alpha = \beta = \gamma = 90°$ for α-HMX, and $\alpha = \beta = 90°$ and $\gamma = 120°$ for δ-HMX, respectively.

The thermal expansion coefficient is an important parameter to characterize the physical and the explosive behavior of the energetic materials. The linear and volume coefficients of β-HMX, α-HMX, and δ-HMX are listed in the Table 2. The average linear coefficients of β-HMX, $6.884 \cdot 10^{-5}$ K^{-1}, agree with the previous experimental result of $5.04 \cdot 10^{-5}$ K^{-1}.[32] There exits a small discrepancy between our results and ref 15 for the different temperature range and space group possibly. Figures 2 to 4 show that the thermal expansion of the β-HMX and α-HMX is weakly anisotropic. Expansions along the crystal axes *b* and *c* are 2.37 % and 2.44 %, respectively; both are slightly

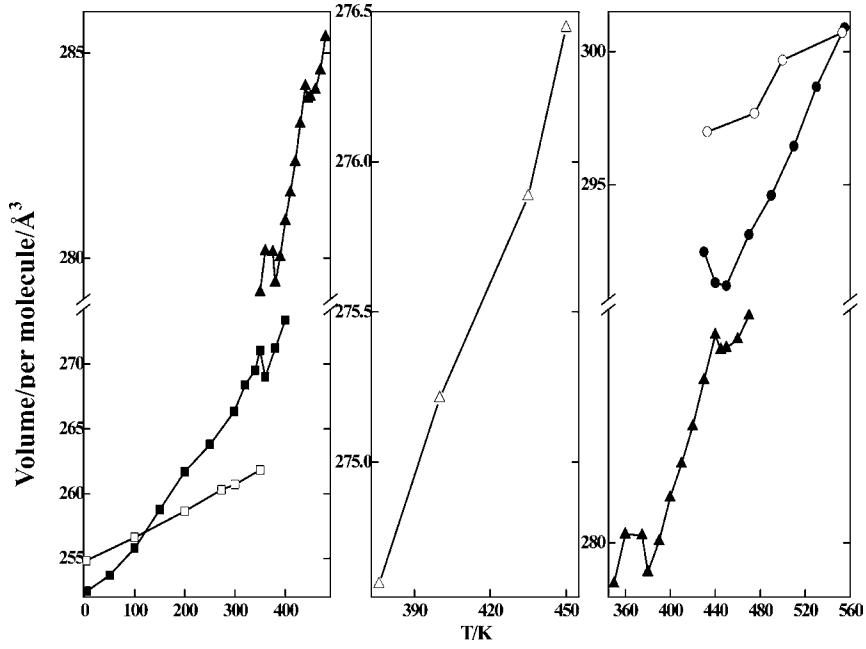

Figure 5. Unit cell volume *V* as a function of temperature for three HMX, 0 GPa, in this work and atmospheric pressure in ref 15. ■, this work (β-HMX); □, ref 15 (β-HMX); ▲, this work (α-HMX); △, ref 15 (α-HMX); ●, this work (δ-HMX), ○, ref 15 (δ-HMX).

Table 2. Thermal Expansion Coefficients χ_i of the β-, α-, and δ-HMX Crystals

		χ_a	χ_b	χ_c	χ_V
		K^{-1}			
β-HMX	this work, (5 to 350) K	$6.709 \cdot 10^{-5}$	$6.882 \cdot 10^{-5}$	$7.061 \cdot 10^{-5}$	$2.130 \cdot 10^{-4}$
	ref 15, (4.2 to 350) K	$2.446 \cdot 10^{-5}$	$4.082 \cdot 10^{-5}$	$1.775 \cdot 10^{-5}$	$8.242 \cdot 10^{-5}$
	ref 31, 298 K	$5.04 \cdot 10^{-5}$	$5.04 \cdot 10^{-5}$	$5.04 \cdot 10^{-5}$	
α-HMX	this work, (375 to 440) K	$7.359 \cdot 10^{-5}$	$6.722 \cdot 10^{-5}$	$7.359 \cdot 10^{-5}$	$2.218 \cdot 10^{-4}$
	ref 15, (376 to 450) K	$3.232 \cdot 10^{-5}$	$4.117 \cdot 10^{-5}$	$1.932 \cdot 10^{-5}$	$8.987 \cdot 10^{-5}$
δ-HMX	this work, (440 to 530) K	$9.276 \cdot 10^{-5}$	$9.276 \cdot 10^{-5}$	$9.275 \cdot 10^{-5}$	$2.806 \cdot 10^{-4}$
	ref 15, (433 to 553) K	$4.139 \cdot 10^{-5}$	$4.002 \cdot 10^{-5}$	$4.864 \cdot 10^{-5}$	$1.170 \cdot 10^{-4}$

larger than that along the *a*-axis (2.31 %) in the temperature range of (5 to 350) K for β-HMX. Furthermore, we found that both linear and volume thermal expansions of the three phases vary slightly with the temperature increasing in their stable temperature range, but the temperature effect on the thermal expansion can be nearly ignored due to the very small amplitude.

Under Different Pressures. Under different pressures, the lattice parameters and volumes under different temperatures are listed in the Figures 6 to 9 for δ-HMX, β-HMX, and α-HMX. From Figures 6 and 9, the lattice parameters and volumes of β-HMX vary nonlinearly with pressure and exhibit an abrupt change at 27 GPa in the pressure range (0 to 31) GPa, which agrees with the results of Yoo and Cynn.[9] From Figures 7 and 9, α-HMX phase exhibits two abrupt changes: at (25 and 38) GPa. From Figures 8 and 9, we found that the δ-HMX phase undergoes two abrupt changes: at (25 and 36) GPa. That is to say, α-HMX and δ-HMX phases are relatively stable in the pressure range of (25 to 38) GPa and (25 to 36) GPa, respectively. It indicates that β-HMX undergoes a phase transition at 27 GPa, in agreement with the experimental[9] and theoretical[16] results. While β-HMX will transit to the α-HMX phase or the δ-HMX phase, it depends on the stability of α-HMX and δ-HMX phases under high pressure. We can estimate it from the total energy of α-HMX and δ-HMX phases in the range of the (25 to 36) GPa. Figure 10 shows that the total energy of δ-HMX phases is lower than that of the α-HMX phase, that is, the δ-HMX phase is the stable phase in the range of (25 to 36) GPa until it can be detonated over 36 GPa, which agrees with the explosive pressure of 39 GPa.[32] Hence, β-HMX exhibits a phase transition to the δ-HMX phases at (25 to 27) GPa. With pressure increasing from (0 to 27) GPa, the lattice parameters and cell volumes decrease, and the crystalline density of β-HMX increases gradually. In the pressure range of (0 to 27) GPa, the ratios of the change of lattice parameters and volumes are 14.4 %, 14.3 %, 15.6 %, and 37.1 % for *a*, *b*, *c*, and *V*, respectively. The ratio of the compression of lattice parameters and volumes of δ-HMX phases are 2.45 % and 7.16 % for *a*, *b*, *c*, and *V*, respectively. The ratio of compression of β-HMX agrees with the experimental results,[9] while there are no corresponding experimental data to compare with δ-HMX in high pressures. The influence of the pressure on the lattice parameters and volumes is larger than the temperature obviously.

Mechanical Properties. The elastic coefficients can be computed by taking the first derivatives of the stress with regard to strain.[33] Each structure is subjected to uniaxial tensile and pure shear deformations, and the induced stress tensors can be obtained from the Virial formalism in atomistic calculations.

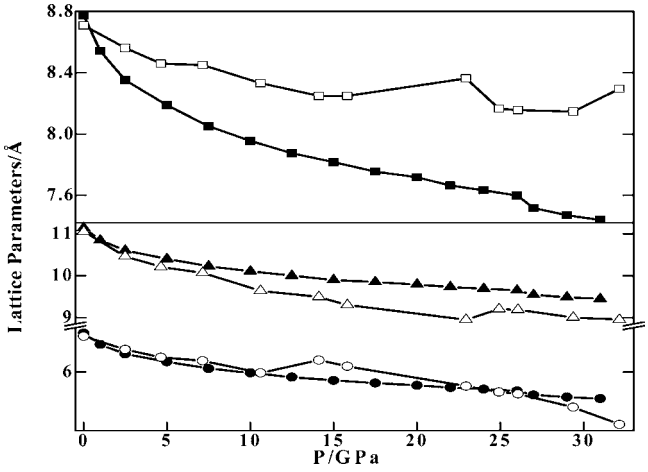

Figure 6. Lattice parameters of β-HMX at different pressures and 298 K, the experimental results from ref 9 at atmospheric conditions. ●, *a* in this work; ○, *a* in ref 9; ▲, *b* in this work; △, *b* in ref 9; ■, *c* in this work; □, *c* in ref 9.

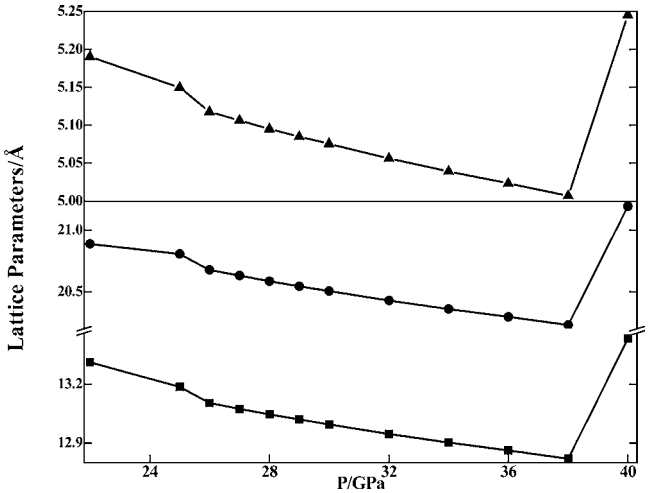

Figure 7. Lattice parameters of α-HMX at different pressures and 298 K. ■, *a* in this work; ●, *b* in this work; ▲, *c* in this work.

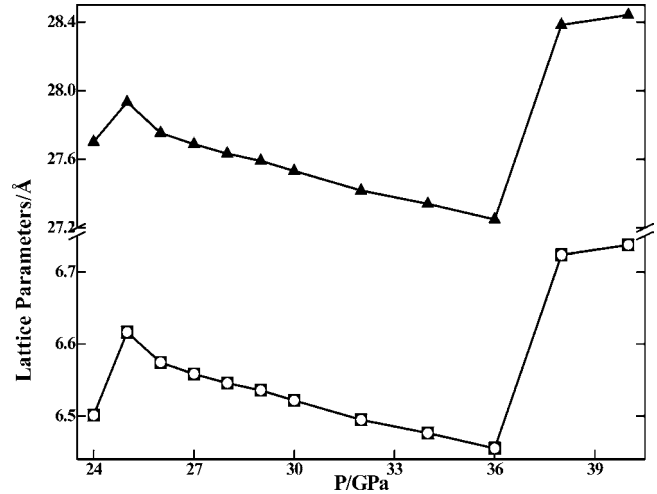

Figure 8. Lattice parameters of δ-HMX at different pressures and 298 K. ■, *a* in this work; ○, *b* in this work; ▲, *c* in this work.

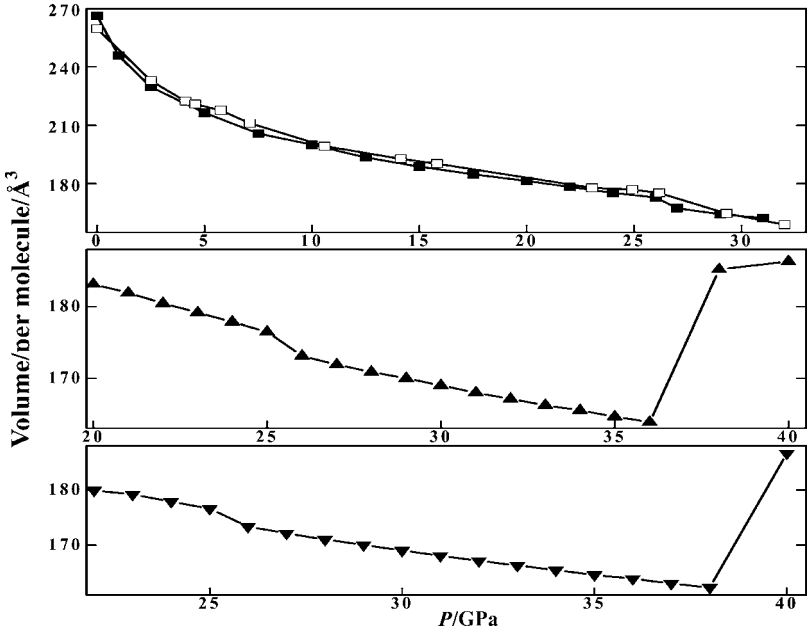

Figure 9. Unit cell volume V as a function of pressure for three HMX at 298 K. ■, this work (β-HMX); □, ref 9 at atmospheric conditions (β-HMX); ▲, this work (δ-HMX); ▼, this work (α-HMX).

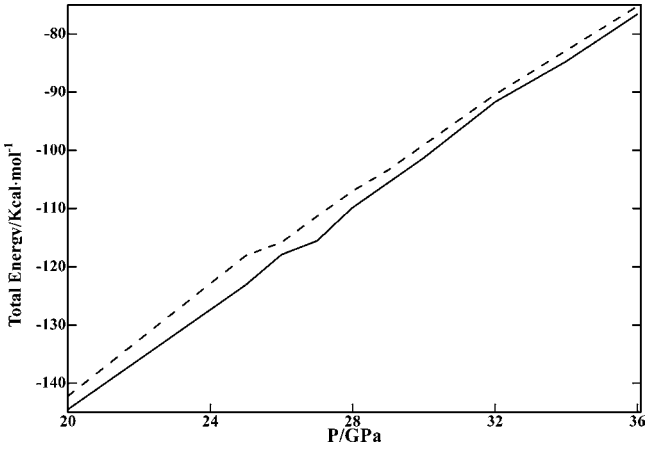

Figure 10. Total energy of the α- and δ-HMX at different pressures and 298 K. ---, α-HMX; —, δ-HMX.

We can obtain the Young's modulus and Poisson ratio from the least-squares fits of the average tensile stress versus tensile strain, respectively. We can also calculate other mechanical parameters such as the bulk modulus, shear modulus, and Lamé coefficients. Here the second-order elastic tensors and various elastic moduli, including the Young's modulus (E), bulk modulus (K), and shear modulus (G) and Poisson's ratio (γ). We computed these mechanical parameters in the range of (5 to 400) K at 0 GPa and the pressure range of (0 to 31) GPa at 298 K for β-HMX, in the range of (350 to 480) K at 0 GPa and the pressure range of (22 to 40) GPa at 298 K for α-HMX, and in the range of (430 to 555) K at 0 GPa and the pressure range of (20 to 40) GPa at 298 K for δ-HMX. All results together with other theoretical and experimental values are presented in Tables 3 to 7, respectively.

Generally speaking, the diagonal elements C_{ii} describe the crystal stiffness under uniaxial compression and shear, while the off-diagonal elements C_{ij} ($i \neq j$) correspond to biaxial compression and distortion of the crystal. From Tables 3 and 4, we found that there is remarkable anisotropy in the diagonal elements C_{ii} ($i = 1$ to 6) of the elastic constant tensor, which can be related to the crystal structure. Therefore, for β-HMX it can be concluded that it is anisotropic upon compression and has a good stability to shear deformation perpendicular to the

Table 3. Elastic Constants and Cauchy Pressure ($C_{12} - C_{44}$) of β-HMX under 0 GPa at Different Temperatures Compared with Other Results[a]

T/K	C_{11}	C_{22}	C_{33}	C_{44}	C_{55}	C_{66}	C_{12}	C_{13}	C_{15}	C_{23}	C_{25}	C_{35}	C_{46}	$C_{12} - C_{44}$
								GPa						
5	22.5	16.4	20.5	9.04	5.15	6.68	6.50	8.47	−0.74	10.7	−4.17	−1.94	−3.32	−2.54
50	21.2	15.4	19.5	8.69	5.00	6.41	6.07	7.89	−0.68	9.89	−3.96	−1.81	−3.15	−2.62
100	19.7	14.2	18.2	8.25	4.81	6.07	5.57	7.22	−0.59	8.90	−3.72	−1.64	−2.94	−2.68
150	18.1	13.0	16.9	7.79	4.63	5.74	5.09	6.54	−0.50	7.90	−3.46	−1.48	−2.73	−2.70
200	16.5	11.7	15.5	7.31	4.42	5.36	4.59	5.85	−0.38	6.85	−3.20	−1.30	−2.51	−2.72
250	15.0	10.6	14.3	6.85	4.23	5.01	4.16	5.23	−0.26	5.93	−2.95	−1.12	−2.30	−2.69
298	13.6	9.50	13.2	6.41	4.04	4.68	3.75	4.66	−0.15	5.07	−2.71	−0.96	−2.10	−2.66
320	13.1	9.18	12.8	6.26	3.99	4.56	3.62	4.48	−0.11	4.80	−2.63	−0.90	−2.04	−2.64
340	12.5	8.71	12.3	6.06	3.90	4.40	3.43	4.24	−0.06	4.43	−2.52	−0.82	−1.95	−2.63
350	12.0	8.30	11.8	5.87	3.82	4.27	3.28	4.01	−0.01	4.11	−2.43	−0.75	−1.88	−2.59
360	11.9	8.23	11.7	5.84	3.80	4.24	3.25	3.98	−0.009	4.05	−2.41	−0.74	−1.86	−2.59
380	11.4	7.88	11.4	5.68	3.74	4.12	3.11	3.79	0.04	3.78	−2.33	−0.68	−1.80	−2.57
400	10.9	7.50	11.0	5.50	3.66	3.99	2.96	3.59	0.08	3.48	−2.24	−0.60	−1.73	−2.54
ref 11	18.4	14.4	12.4	4.8	4.8	4.5	6.4	10.5	−1.1	6.4	0.8	1.1	2.8	1.6
ref 14	22.2	23.9	23.4	9.2	11.1	10.0	9.6	13.2	−0.1	13.0	4.7	1.6	2.5	0.4
ref 34	12.8	10.9	11.4	5.9	4.6	4.8	3.4	4.9	−0.4	5.2	−2.7	−0.4	−1.8	−2.5
ref 35	19.4	17.5	17.8	9.1	9.2	9.8	5.9	8.4	−1.1	8.2	0.83	0.2	2.4	−3.2
ref 36	20.8	26.9	18.5	4.2	6.1	2.5	4.8	12.5	−0.5	5.8	−1.9	1.9	2.9	0.6

[a] Stevens and Eckhardt, 2005,[11] at 293 K and 1 atm; Sewell et al., 2003;[14] Sewell et al., 2001;[35] Zaug, 1998,[36] at 295 K and 1 atm.

Table 4. Theoretical Elastic Constants and Cauchy Pressure ($C_{12} - C_{44}$) of β-HMX at 298 K and Different Pressures[a]

P/GPa	C_{11}	C_{22}	C_{33}	C_{44}	C_{55}	C_{66}	C_{12}	C_{13}	C_{15}	C_{23}	C_{25}	C_{35}	C_{46}	$C_{12} - C_{44}$
								GPa						
0	13.6	9.50	13.2	6.41	4.04	4.68	3.75	4.66	−0.15	5.07	−2.71	−0.96	−2.1	−2.66
5	67.9	49.6	52.8	19.5	11.3	14.9	27.9	30.6	−0.97	37.8	−11.3	−6.6	−8.1	8.4
10	102.9	77.9	80.7	28.9	18.6	23.5	53.7	44.9	−2.1	44.9	−18.8	−13.9	−13.5	24.8
15	127.9	102.4	107.0	38.7	28.4	33.8	75.1	52.9	0.16	86.3	−28.6	−19.8	−19.5	36.4
20	158.2	124.5	133.8	44.4	35.7	40.5	90.4	70.0	7.69	104.5	−32.1	−19.4	−21.8	46
25	177.9	153.3	155.0	36.8	35.9	33.6	112.5	103.3	13.2	119.2	−24.5	−12.0	−10.8	75.7
27	191.7	162.4	162.5	34.7	38.6	33.4	120.9	111.7	13.5	125.4	−21.8	−8.2	−6.8	86.2
30	194.8	193.1	184.5	28.9	28.9	31.9	126.5	129.5	11.1	132.6	−12.0	1.37	0.78	97.6
ref 11	18.4	14.4	12.4	4.8	4.8	4.5	6.4	10.5	−1.1	6.4	0.8	1.1	2.8	1.6

[a] Stevens and Eckhardt, 2005,[11] at 293 K and 1 atm.

Table 5. Theoretical Elastic Constants and Cauchy Pressure ($C_{12} - C_{44}$) of α-HMX at 0 GPa, Different Temperatures and 298 K, Different Pressures[a]

T/K	C_{11}	C_{22}	C_{33}	C_{44}	C_{55}	C_{66}	C_{12}	C_{13}	C_{23}	$C_{12} - C_{44}$
						GPa				
350	12.79	13.99	18.01	3.01	−0.203	0.059	3.048	5.411	2.878	0.038
375	12.32	13.2	17.72	2.95	−0.007	0.118	2.801	5.048	2.679	−0.149
380	12.34	13.47	17.49	3.051	0.007	0.156	3.176	4.891	2.727	0.125
390	11.89	12.97	17.03	2.971	0.169	0.308	2.681	4.735	2.322	−0.29
420	11.35	12.16	16.82	2.704	0.049	0.282	2.917	4.394	2.046	0.213
440	11.41	11.93	16.55	2.763	0.317	0.213	2.758	4.497	1.875	−0.005
445	10.98	11.69	16.08	2.488	0.216	0.180	2.598	4.298	1.699	0.11
460	10.87	11.22	16.40	2.892	0.171	0.283	2.578	4.307	1.337	−0.314
480	10.73	10.65	15.83	2.340	0.343	0.299	2.391	3.986	1.421	0.051
ref 14	30.6	23.3	31.4	0.80	3.3	3.3	5.7	13.8	6.0	
P/GPa										
27	193.2	184.4	184.3	26.68	27.35	19.08	108.7	116.7	115.9	82.02
30	197.8	199.3	197.6	28.18	30.44	21.25	120.9	126.5	129.2	92.72
32	205.6	210.0	204.0	32.90	32.85	26.73	137.8	135.8	132.0	104.90
34	221.8	214.8	222.7	32.57	33.00	26.18	134.0	142.0	142.4	101.43
36	226.4	224.0	214.1	38.63	34.04	26.50	139.2	153.2	155.0	100.57

[a] Sewell et al., 2003,[14] at 295 K and 1 atm.

c-axis. Most of the elastic constants decrease with increasing temperature from (5 to 360) K and increase with increasing pressure in the range of (0 to 31) GPa. The alterations for the constants C_{11}, C_{22}, and C_{33} and the off-diagonal elements C_{12}, C_{13}, and C_{23} are especially remarkable, whereas those for the shear constants C_{55} and C_{66} are less pronounced in its stable temperature and pressure range. On the contrary, the change rules of C_{15}, C_{25}, C_{35}, and C_{46} are not remarkable. Our results agree with other theoretical[14,34] and experimental[11,35,36] results within the similar temperature range. From Table 5, most of the elastic constants of α-HMX decrease with the increasing temperature and increase with the increasing pressure except for C_{55} and C_{66} in the temperature range (375 to 440) K and in the pressure range (22 to 36) GPa. From Table 6, in the stable conditions of δ-HMX we found that all of the elastic constants decrease with increasing temperature and increase with increasing pressure until its explosive temperature and pressure.[32] These results suggest that HMX crystal rigidity decreases and the anisotropy is enhanced with increasing temperature and is weakened with increasing pressure slightly. From Tables 3 to 6, we found that the effect of pressure on the elastic constants is larger than the effect of the temperature, which agrees with the former results.

As we all know, the Cauchy pressure ($C_{12} - C_{44}$) can be used to evaluate the ductibility or brittleness of a material.[37] The ($C_{12} - C_{44}$) value of a ductile material is positive, whereas the negative value corresponds to a brittle material. The larger positive ($C_{12} - C_{44}$) value of a material, the more ductile this material is. The ($C_{12} - C_{44}$) data are given in Tables 3 to 6. It is shown that β-HMX and δ-HMX are brittle materials with

Table 6. Theoretical Elastic Constants and Cauchy Pressure ($C_{12} - C_{44}$) of δ-HMX at 0 GPa, Different Temperatures and 298 K, Different Pressures[a]

T/K	$C_{11} = C_{22}$	C_{33}	$C_{44} = C_{55}$	C_{12}	$C_{13} = C_{23}$	$C_{12} - C_{44}$
			GPa			
430	6.328	9.884	3.327	2.244	4.334	−1.083
450	5.912	9.099	3.142	1.907	3.771	−1.235
470	5.702	8.944	3.151	2.101	3.595	−1.050
490	5.589	8.030	2.925	1.929	3.317	−0.996
510	5.369	7.949	2.981	1.492	3.160	−1.489
530	4.921	7.902	2.692	1.564	3.389	−1.128
ref 14	14.5	14.0	4.4	10.3	10.3	
P/GPa						
25	163.8	163.6	26.38	111.1	114.4	84.72
28	182.2	177.6	26.77	122.1	121.1	95.33
30	184.5	197.8	32.18	130.2	134.0	101.82
32	191.3	203.5	35.86	132.8	138.1	102.24
34	213.3	211.5	36.74	142.3	144.4	107.66
35	224.1	220.9	38.22	144.7	144.6	106.38
36	222.3	226.6	38.50	148.2	150.7	109.70
38	123.1	114.7	16.82	85.69	80.14	68.87

[a] Sewell et al., 2003,[14] at 295 K and 1 atm.

negative ($C_{12} - C_{44}$) at high temperatures and are ductile materials in high pressure. Hence, we can change the relevant properties of HMX by changing the pressure and temperature.

Table 7 lists the mechanical properties of β-, α-, and δ-HMX under different temperatures at 0 GPa and different pressures at 298 K, that is, Young's modulus *E*, bulk modulus *K*, shear modulus *G*, Poisson's ratio γ, Lamé coefficients λ and μ, and *K*/*G* ratio. All of the isotropic moduli of β-HMX, α-HMX, and δ-HMX decrease gradually with increasing temperature and increase with increasing pressure, thus the

Table 7. Mechanical Properties of β-, α-, and δ-HMX Crystal under 0 GPa, Different Temperatures and 298 K, Different Pressures[a]

		Young's modulus	bulk modulus	shear modulus	Poisson's ratio	Lamé coefficient	Lamé coefficient	ratio of K
	T/K	E	K	G	γ	π	μ	K/G
					GPa			
β-HMX	5	14.65	12.30	5.626	0.3016	8.553	5.626	2.186
	50	13.96	11.53	5.375	0.2983	7.950	5.375	2.145
	100	13.11	10.61	5.066	0.2940	7.228	5.066	2.094
	150	12.23	9.672	4.745	0.2892	6.509	4.475	2.038
	200	11.30	8.696	4.403	0.2834	5.761	4.403	1.975
	250	10.45	7.834	4.091	0.2776	5.107	4.091	1.915
	298	9.646	7.021	3.794	0.2710	4.492	3.794	1.851
	320	9.388	6.768	3.699	0.2688	4.302	3.699	1.830
	340	9.025	6.412	3.566	0.2654	4.035	3.566	1.798
	350	8.706	6.099	3.449	0.2621	3.800	3.449	1.768
	360	8.649	6.043	3.428	0.2614	3.757	3.428	1.763
	380	8.379	5.778	3.330	0.2583	3.558	3.330	1.735
	400	8.081	5.492	3.220	0.2547	3.345	3.220	1.706
	ref 11		9.6	3.1				3.097
	ref 14		15.1	7.0				2.157
	ref 35		6.9	3.6	0.3			1.917
	ref 36		12.5	1.3				9.615
	P/GPa							
	0	9.646	7.021	3.794	0.2710	4.492	3.794	1.851
	5	33.60	40.31	12.34	0.3611	32.08	12.34	3.267
	10	45.66	65.16	16.51	0.3832	54.15	16.21	3.947
	15	56.94	85.08	20.51	0.3885	71.41	20.51	4.148
	20	68.93	105.8	24.77	0.3914	89.27	24.77	4.271
	25	71.04	128.5	25.23	0.4079	111.7	25.23	5.093
	27	74.46	137.0	26.41	0.4094	119.4	26.41	5.187
	30	86.05	149.9	30.64	0.4044	129.5	30.64	4.892
	T/K							
α-HMX	350	13.44	7.466	5.600	0.2000	3.732	5.600	1.333
	375	13.04	7.143	5.453	0.1958	3.508	5.453	1.310
	380	13.02	7.187	5.432	0.1981	3.565	5.432	1.323
	390	12.69	6.863	5.325	0.1917	3.312	5.325	1.289
	420	12.26	6.571	5.156	0.1890	3.134	5.156	1.274
	440	12.23	6.390	5.179	0.1809	2.937	5.179	1.234
	445	11.90	6.191	5.045	0.1796	2.828	5.045	1.227
	460	11.95	6.023	5.108	0.1694	2.617	5.108	1.179
	480	11.56	5.801	4.952	0.1677	2.499	4.952	1.171
	ref 14		14.1	2.4				5.875
	P/GPa							
	0	9.646	7.021	3.794	0.2710	4.492	3.794	1.851
	5	33.60	40.31	12.34	0.3611	32.08	12.34	3.267
	10	45.66	65.16	16.51	0.3832	54.15	16.21	3.947
	15	56.94	85.08	20.51	0.3885	71.41	20.51	4.148
	20	68.93	105.8	24.77	0.3914	89.27	24.77	4.271
	25	71.04	128.5	25.23	0.4079	111.7	25.23	5.093
	27	74.46	137.0	26.41	0.4094	119.4	26.41	5.187
	30	86.05	149.9	30.64	0.4044	129.5	30.64	4.892
	T/K							
δ-HMX	430	5.069	4.931	1.908	0.3286	3.659	1.908	2.584
	450	5.031	4.433	1.919	0.3109	3.514	1.919	2.310
	470	4.676	4.297	1.773	0.3186	3.115	1.773	2.424
	490	4.685	4.114	1.788	0.3102	2.922	1.788	2.301
	510	4.659	3.830	1.796	0.2972	2.633	1.796	2.133
	530	4.199	3.705	1.601	0.3111	2.638	1.601	2.314
	ref 14		11.8	2.9				4.069
	P/GPa							
	25	69.58	129.1	24.67	0.4102	112.7	24.67	5.233
	28	80.44	140.5	28.64	0.4046	121.4	28.64	4.906
	30	84.48	151.5	30.01	0.4065	130.5	30.01	5.048
	32	90.94	156.7	32.40	0.4033	135.1	32.40	4.836
	34	97.34	164.7	34.73	0.4015	141.5	34.73	4.742
	35	105.4	170.7	37.74	0.3971	145.6	37.74	4.523
	36	102.0	173.2	36.40	0.4018	149.0	36.40	4.758
	38	53.67	93.4	19.11	0.4041	80.5	19.11	4.887

[a] Stevens and Eckhardt, 2005,[11] at 293 K and 1 atm; Sewell et al., 2003;[14] Sewell et al.;[35] Zaug, 1998,[36] at 295 K and 1 atm.

rigidity and brittleness of the HMX decrease. It can be seen that at the low temperatures and low pressures, β-HMX has large stiffness, plasticity, and fracture strength to resist the external stress. Compared with β-HMX, δ-HMX has smaller stiffness, plasticity, and fracture strength to resist the external stress at different temperature. This indicates that the β-HMX will deform more easily when it is subjected to external loading at a higher temperature. While at higher pressures, the δ-HMX will deform more easily than β-HMX. Such a result can be understood by the following two reasons: (1) the internal free volume is expanded more severely with the increasing temperature and decreasing pressure, and (2) the molecules within the crystal gain more kinetic energies when the temperature rises. It is interesting that the change of shear modulus is smaller than those for the Young's modulus and bulk modulus with the change of temperature and pressure.

This consists of less changes in the shear constants C_{55} and C_{66} with changing temperature and pressure. Hence, we suggested that β-HMX and δ-HMX possess good stability for shear loading in the temperature range of their stable temperatures. The Poisson's ratio correlates various isotropic moduli through the formula $E = 3K(1 - 2\gamma) = 2G(1 + \gamma)$. We can estimate the plasticity of a material from the Poisson's ratio. In general, the Poisson's ratio of a plastic is 0.2 to 0.4. The Poisson's ratio decreases from 0.3016 to 0.2614 as the temperature rises from (5 to 360) K or increases from 0.271 to 0.3914 in the pressure range (0 to 20) GPa for β-HMX. The Poisson's ratio of α-HMX increases from 0.3778 to 0.3883 with the pressure rise from (27 to 34) GPa. For δ-HMX, the Poisson's ratio decreases from 0.3286 to 0.2972 as the temperature increases from (430 to 510) K. These results suggest that β-HMX in the range (5 to 360) K and in the (0 to 20) GPa range, α-HMX in the range (27 to 34) GPa, and δ-HMX in the temperature range (430 to 510) K exhibit plasticity.

Moreover, the extent of the plastic range for a material can be estimated by the ratio of the bulk modulus to shear modulus, that is, K/G.[38] A higher K/G value denotes more malleability, and a lower value means brittleness.[38] In Table 7, it can be deduced that the β-HMX at lower temperatures and higher pressures, the α-HMX at higher pressures, and the δ-HMX at lower temperatures have better malleability, which agrees well with the conclusion drawn from the Cauchy pressure (C_{12} to C_{14}).

Conclusions

In this paper, MD simulations are performed to study phase transition and mechanical properties of the energetic material of β-, α-, and δ-HMX. The effects of pressure and temperature on the structures and mechanical properties are discussed. The crystal structure of β-, α-, and δ-HMX from COMPASS force field simulations compares reasonably with experiments. In the range of the simulated temperature and pressure, the lattice parameters and volumes show nonlinear dependence on the temperature and pressure. Under high temperatures, there exist two phase transitions, that is, from β- to α-HMX at 360 K and from α- to δ-HMX at 440 K. Under high pressures, the β-HMX transit to δ-HMX at 27 GPa. Within the effective range of temperature and pressure, it can be deduced that β-HMX at lower temperatures and higher pressures, α-HMX at higher pressures, and δ-HMX at lower temperatures have better malleability. We expect our results be helpful for understanding the behavior of HMX at high temperatures and pressures.

Literature Cited

(1) Cooper, P. W.; Kurowski, S. R. *Introduction to the Technology of Explosives*; Wiley: New York, 1996.

(2) Cady, H. H.; Smith, L. C. *Studies on the Polymorphs of HMX*; Los Alamos Scientific Laboratory Report LAMS-2652 TID-4500; Los Alamos National Laboratory: Los Alamos, NM, 1961.

(3) Goetz, F.; Brill, T. B.; Ferraro, J. R. Pressure Dependence of the Raman and Infrared Spectra of α-, β-, γ- and δ-octahydro-1,3,5,7-tetranitro-1,3,5,7-tetrazocine. *J. Phys. Chem.* **1978**, *82*, 1912–1917.

(4) Main, P.; Cobbledick, R. E.; Small, R. W. H. Structure of the Fourth Form of 1,3,5,7-tetranitro-1,3,5,7-tetraazacyclooctane (γ-HMX), $2C_4H_8N_8O_8 \cdot 0.5H_2O$. *Acta Crystallogr., Sect. C* **1985**, *41*, 1351–1354.

(5) Cady, H. H.; Larson, A. C.; Cromer, D. T. The Crystal Structure of α-HMX and a Refinement of the Structure of β-HMX. *Acta Crystallogr.* **1963**, *16*, 617–623.

(6) Choi, C. S.; Boutin, H. P. A. Study of the Crystal Structure of β-cyclotetra-methylene tetranitramine by neutron diffraction. *Acta Crystallogr., Sect. B* **1970**, *26*, 1235–1240.

(7) Landers, A. G.; Brill, T. B. Pressure-Temperature Dependence of the β-δ Polymorph Interconversion in Octahydro-1,3,5,7-tetranitro-1,3,5,7-tetrazocine. *J. Phys. Chem.* **1980**, *84*, 3573–3577.

(8) Cobbledick, R. E.; Small, R. W. H. The Crystal Structure of the δ-form of 1,3,5,7- tetranitro-1,3,5,7-tetraazacyclooctane (δ-HMX). *Acta Crystallogr., Sect. B* **1974**, *30*, 1918–1922.

(9) Yoo, C. S.; Cynn, H. Equation of State, Phase Transition, Decomposition of β-HMX (octahydro-1,3,5,7- tetranitro-1,3,5,7-tetrazocine) at High Pressures. *J. Chem. Phys.* **1999**, *111*, 10229–10235.

(10) Gump, J. C.; Peiris, S. M. Isothermal Equations of State of beta octahydro-1,3,5,7-tetranitro-1,3,5,7-tetrazocine at High Temperatures. *J. Appl. Phys.* **2005**, *97*, 053513−053519.

(11) Stevens, L. L.; Eckhardt, C. J. The Elastic Constants and Related Properties of β-HMX Determined by Brillouin Scattering. *J. Chem. Phys.* **2005**, *122*, 174701–174708.

(12) Parrinell, M.; Rahman, A. Polymorphic Transitions in Single Crystals: A New Molecular Dynamics Method. *J. Appl. Phys.* **1981**, *52*, 7182–7190.

(13) Sewell, T. D. Monte Carlo Calculations of the Hydrostatic Compression of Hexahydro-1,3,5-trinitro-1,3,5-triazine and β-octahydro-1,3,5,7-tetranitro-1,3,5,7-tetrazocine. *J. Appl. Phys.* **1998**, *83*, 4142–4145.

(14) Sewell, T. D.; Menikoff, R.; Bedrov, D.; Smith, G. D. A Molecular Dynamics Study of Elastic Properties of HMX. *J. Chem. Phys.* **2003**, *119*, 7417–7426.

(15) Sorescu, D. C.; Rice, B. M.; Thompson, D. L. Isothermal-Isobaric Molecular Dynamics Simulations of 1,3,5,7-Tetranitro-1,3,5,7-Tetraazacyclooctane (HMX) Crystals. *J. Phys. Chem.* **1998**, *102*, 6692–6695.

(16) Lu, L. Y.; Wei, D. Q.; Chen, X. R.; Ji, G. F.; Wang, X. J.; Chang, J.; Zhang, Q. M.; Gong, Z. Z. The Pressure-induced Phase Transition of the Solid β-HMX. *Mol. Phys.* **2009**, *107*, 2373–2385.

(17) Lewis, J. P.; Sewell, T. D.; Evans, R. B.; Voth, G. A. Electronic Structure Calculation of the Structures and Energies of the three Pure Polymorphic Forms of Crystalline HMX. *J. Phys. Chem. B* **2000**, *104*, 1009–1013.

(18) Byrd, E. F. C.; Rice, B. M. Ab Initio Study of Compressed 1,3,5,7-Tetranitro-1,3,5,7-Tetraazacyclooctane (HMX), Cyclotrimethylenetrinitramine (RDX), 2,4,6,8,10,12-Hexanitrohexaazaisowurzitane (CL-20), 2,4,6-Trinitro-1,3,5-benzenetriamine (TATB) and Pentaerythritol Tetranitrate (PETN). *J. Phys. Chem. C* **2007**, *111*, 2787–2796.

(19) Zhu, W. H.; Xiao, J. J.; Ji, G. F.; Zhao, F.; Xiao, H. M. First-Principles Study of the Four Polymorphs of Crystalline Octahydro-1,3,5,7-tetranitro-1,3,5,7-tetrazocine. *J. Phys. Chem. B* **2007**, *111*, 12715–12722.

(20) Lu, L. Y.; Wei, D. Q.; Chen, X. R.; Ji, G. F.; Zhang, Q. M.; Gong, Z. Z. The Structural Properties of Solid β-HMX under Compression by the First Principle Study. *Mol. Phys.* **2008**, *106*, 2569–2580.

(21) Zerilli, F. J.; Kuklja, M. M. Ab initio Equation of State for β-HMX. *Shock Compression Condens. Matter* **2007**, *CP955*, 437–440.

(22) *Materials Studio 4.0*; Accelrys, Inc.: San Diego, CA, 2006.

(23) Sun, H. COMPASS: An ab Initio Force-Field Optimized for Condensed-Phase Applications-Overview with Details on Alkane and Benzene Compounds. *J. Phys. Chem. B* **1998**, *102*, 7338–7364.

(24) Berendsen, H. J. C.; Postma, J. P. M.; Van Gunsteren, W. F.; DiNola, A.; Haak, J. R. Molecular Dynamics with Coupling to an External Bath. *J. Chem. Phys.* **1984**, *81*, 3684–3690.

(25) Andersen, H. C. Molecular Dynamics Simulations at Constant Pressure and/or Temperature. *J. Chem. Phys.* **1980**, *72*, 2384–2393.

(26) Allen, M. P.; Tindesley, D. J. *Computer Simulation of Liquids*; Oxford University Press: New York, 1989.

(27) Xu, X. J.; Xiao, H. M.; Gong, X. D.; Ju, X. H.; Chen, Z. X. Theoretical Studies on the Vibrational Spectra, Thermodynamic Properties, Detonation Properties, and Pyrolysis Mechanisms for Polynitroadamantanes. *J. Phys. Chem. A* **2005**, *109*, 11268–11274.

(28) Qiu, L.; Zhu, W. H.; Xiao, J. J.; Xiao, H. M. Theoretical Studies of Solid Bicyclo-HMX: Effects of Hydrostatic Pressure and Temperature. *J. Phys. Chem. B* **2008**, *112*, 3882–3893.

(29) Xu, X. J.; Xiao, H. M.; Xiao, J. J.; Zhu, W.; Huang, H.; Li, J. S. Molecular Dynamics Simulations for Pure ε-CL-20 and ε-CL-20-Based PBXs. *J. Phys. Chem. B* **2006**, *110*, 7203–7207.

(30) Qiu, L.; Xiao, H. M.; Zhu, W. H.; Xiao, J. J.; Zhu, W. Ab Initio and Molecular Dynamics Studies of Crystalline TNAD (trans-1,4,5,8-Tetranitro-1,4,5,8-tetraazadecalin). *J. Phys. Chem. B* **2006**, *110*, 10651–10661.

(31) Qiu, L.; Zhu, W. H.; Xiao, J. J.; Zhu, W.; Xiao, H. M.; Huang, H.; Li, J. S. Molecular Dynamics Simulations of Trans-1,4,5,8-tetranitro-1,4,5,8-tetraazadecalin-Based Polymer-Bonded Explosives. *J. Phys. Chem. B* **2007**, *111*, 1559–1566.

(32) Dong, H. S.; Zhou, F. F. *Performance of High Energetic Explosive and Related Compounds* (in Chinese); Science Press: Beijing, 1989.
(33) Weiner, J. H. *Statistical Mechanics of Elasticity*; John Wiley and Sons: New York, 1983; Sec.6.10.
(34) Xiao, J. J.; Fang, G. Y.; Ji, G. F.; Xiao, H. M. Simulation Investigations in the Binding Energy and Mechanical Properties of HMX-based Polymer-bonded Explosives. *Chin. Sci. Bull.* **2005**, *50*, 21–26.
(35) Sewell, T. D.; Bedrov, D.; Menikoff, R.; Smith, G. D. Elastic Properties of HMX. *Shock Compression Condens. Matter* **2002**, *620*, 399–402.
(36) Zaug, J. M. In *Elastic Constants of β-HMX and Tantalum, Equations of State of Supercritical Fluids and Fluid Mixtures and Thermal Transport Determinations*, Proceedings of 11th International Detonation Symposium, Snowmass, CO, 1998; p 498.
(37) Pettifor, D. G. Theoretical Predictions of Structure and Related Properties of Inter-metallics. *Mater. Sci. Technol.* **1992**, *8*, 345–349.
(38) Pugh, S. F. Relation Between the Elastic Moduli and the Plastic Properties of Polycrystalline Pure Metals. *Philos. Mag. A* **1954**, *45*, 823–843.

Received for review January 6, 2010. Accepted March 11, 2010. We acknowledge the support for this work by the National Key Laboratory Fund for Shock Wave and Detonation Physics Research of the China Academy of Engineering Physics under Grant No. 9140C6711010805, the National Science Foundation of China under the Contract No. 20773085, the State Key Laboratory of Explosion Science and Technology, Beijing Institute of Technology under Grant KFJJ09-02, the "National Basic Research Program of China" (No. 2010CB731600), as well as Rui-Feng Co. and the Virtual Laboratory for Computational Chemistry of CNIC, and the Supercomputing Center of CNIC, Chinese Academy of Science.

JE100009M